Stability and bifurcation behaviour of electrostatic torsional NEMS varactor influenced by dispersion forces

Wen-Hui Lin[1] and Ya-Pu Zhao[2,3]

[1] College of Science, China Agricultural University, Beijing 100083, People's Republic of China
[2] State Key Laboratory of Nonlinear Mechanics (LNM), Institute of Mechanics, Chinese Academy of Sciences, Beijing 100080, People's Republic of China

E-mail: yzhao@lnm.imech.ac.cn

Abstract
The influences of Casimir and van der Waals forces on the nano-electromechanical systems (NEMS) electrostatic torsional varactor are studied. A one degree of freedom, the torsional angle, is adopted, and the bifurcation behaviour of the NEMS torsional varactor is investigated. There are two bifurcation points, one of which is a Hopf bifurcation point and the other is an unstable saddle point. The phase portraits are also drawn, in which periodic orbits are around the Hopf bifurcation point, but the periodic orbit will break into a homoclinic orbit when meeting the unstable saddle point.

1. Introduction

It has been recognized recently that vacuum-induced forces play considerable roles in micro-, nano- and quantum-electromechanical systems (MEMS, NEMS and QEMS) with typical sizes in the micrometre range or below [1–6]. Actuation, pull-in and stiction/adhesion are the three major concerns for the application of Casimir and van der Waals (vdW) forces in MEMS or NEMS [1–21].

It is well known that both vdW and Casimir forces are connected with the existence of zero-point vacuum oscillations of the electromagnetic field [22]. For closely spaced macroscopic bodies, the virtual photon emitted by an atom of one body reaches an atom of the second body during its lifetime. The nonretarded vdW force arises from the correlated oscillations of the instantaneously induced dipole moments of those atoms. The Casimir force, also known as the retarded vdW force, arises when the distance between the two bodies is so large that the virtual photons emitted by an atom of one body cannot reach the second body during its lifetime. This retardation effect due to the finite speed of light causes the scaling behaviour of the dispersion force to change from $1/(\text{distance})^3$ for the vdW force to $1/(\text{distance})^4$ for the

Casimir force. Further discussion on the relation between these two forces is referred to in [20]. The vdW and Casimir forces are electromagnetic in nature, and they modify bulk properties such as surface tension and capillary effects. There are some practical challenges for the measurement of the Casimir force, namely, the thermal effect and the surface properties including surface roughness, dielectric properties and finite conductivity of metal surfaces, etc. A general form of the Casimir force has been suggested for different modifications of the material type, temperature and geometry [23]:

$$F = \eta_{\mathrm{m}} \eta_{\mathrm{T}} \eta_{\mathrm{g}} (1 + \Delta_{\mathrm{corr}}) F_0, \tag{1}$$

where

$$F_0 = -\frac{\pi^2}{240} \frac{\hbar c}{H^4} A \tag{2}$$

is the Casimir force between ideal metallic and parallel flat surfaces of area A and distance H at zero temperature with $\hbar$ being Planck's constant divided by 2π and c being the speed of light, $\eta_{\mathrm{m}} < 1$ is the material-dependent factor accounting for the finite conductivity of the plates, $\eta_{\mathrm{T}} > 1$ is the temperature-dependent factor and there is a crossover to a regime with thermal fluctuation becoming relevant for distances H around

---

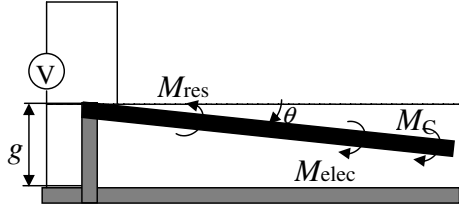[3] Author to whom any correspondence should be addressed.

Figure 1. Schematic of torsional varactor.

the de Broglie wavelength of photons

$$\lambda_T = \frac{\hbar c}{k_B T} \approx 7 \, \mu m, \tag{3}$$

at $T = 300 \, K$ with k_B being the Boltzmann constant, η_g is the geometry-dependent factor accounting for the geometries different from planar parallel plates and Δ_{corr} is the term accounting for the correlations between different modifications. If the distance satisfies $H \ll c/\omega_0$ [24], where ω_0 is the smallest resonance (absorption) frequency of the dielectric and usually $c/\omega_0 \approx$ 5–100 nm, the attractive force between the two plates is the nonretarded vdW force $F_0/A \sim H^{-3}$.

Recently, a MEMS varactor using torsional beams for actuation has been proposed [25]; it has been demonstrated by [25] that the proposed varactor outperforms the other structures in terms of a wide dynamic range and a lower actuation voltage. It is easy to imagine that when the MEMS torsional varactor is miniaturized to a NEMS torsional varactor, the dispersion forces should be considered for actuation and pull-in behaviours when the gap is less than the de Broglie wavelength of photons at room temperature in equation (3). To gain a better understanding of the mechanical behaviour of NEMS varactors, the present paper analysed the influences of both Casimir and van der Waals forces on the pull-in stability of NEMS torsional varactors.

2. Influence of Casimir force

2.1. Mechanical model

For simplicity and without loss of generality, we discuss the torsional varactor shown in figure 1. There is only one degree of freedom, the torsional angle, θ. The restoring torque, $M_{res}(\theta)$, varies linearly with the torsional angle, that is,

$$M_{res}(\theta) = k\theta, \tag{4}$$

where k is the effective spring stiffness [26].

Using the same method as [10], the electrostatic torque is

$$M_{elec}(\theta) = \frac{\varepsilon_0 w V^2}{2\theta^2} \left[\ln\left(\frac{g - L\theta}{g}\right) + \frac{L\theta}{g - L\theta} \right], \tag{5}$$

where w is the width of the beam, L is the length of the beam, g is the initial gap distance when the upper beam is parallel to the ground plane, ε_0 is the dielectric constant and V is the applied voltage.

Now, we compute the Casimir torque in the torsional varactor. Using the same result in [12], we get the Casimir differential force

$$dF_C = \frac{\pi^2 \hbar c w \, dx}{240(g - x\theta)^4}. \tag{6}$$

Then the corresponding torque of the Casimir force is

$$M_C(\theta) = \int_0^L x \cdot dF_C = \frac{\pi^2 \hbar c w L^2}{1440 g^2} \frac{3g - L\theta}{(g - L\theta)^3}. \tag{7}$$

The direction of both the electrostatic and Casimir torques are contrary to that of the restoring torque shown in figure 1. Thus, we obtain the equation of motion as follows:

$$I_0 \frac{d^2\theta}{dt^2} = M_{elec} + M_C - M_{res}, \tag{8}$$

that is,

$$I_0 \frac{d^2\theta}{dt^2} = \frac{\varepsilon_0 w V^2}{2\theta^2} \left[\ln\left(\frac{g - L\theta}{g}\right) + \frac{L\theta}{g - L\theta} \right]$$
$$+ \frac{\pi^2 \hbar c w L^2}{1440 g^2} \frac{3g - L\theta}{(g - L\theta)^3} - k\theta, \tag{9}$$

where I_0 is the moment of inertia. We introduce six dimensionless variables:

(a) $\alpha = \theta/\theta_{max}$, the dimensionless torsional angle;
(b) $\theta_{max} = g/L$, the dimensionless length;
(c) $\tau = t/t_0$, the dimensionless time and t_0 being the characteristic time;
(d) $I = I_0/(kt_0^2)$, the order of magnitude of the ratio between the inertia moment and the restoring torque;
(e) $a = \varepsilon_0 w V^2 L^3/(2kg^3)$, the order of magnitude of the ratio between the electrostatic and the restoring torques;
(f) $b = \pi^2 \hbar c w L^3/(1440 k g^5)$, the order of magnitude of the ratio between the Casimir and the restoring torques.

Then we transform the above equation into a dimensionless form:

$$I \frac{d^2\alpha}{d\tau^2} = \frac{a}{\alpha^2} \left[\ln(1 - \alpha) + \frac{\alpha}{1 - \alpha} \right] + b \frac{3 - \alpha}{(1 - \alpha)^3} - \alpha. \tag{10}$$

According to the definition of these parameters, physically meaningful solutions exist in the region $0 < \alpha < 1$.

2.2. Pull-in parameters

Setting zero the left-hand side of equation (10), we have an equivalent equation as

$$f(\alpha, a, b) = a \left[\ln(1 - \alpha) + \frac{\alpha}{1 - \alpha} \right]$$
$$+ b\alpha^2 \frac{3 - \alpha}{(1 - \alpha)^3} - \alpha^3 = 0. \tag{11}$$

By the critical condition $\partial f(\alpha)/\partial \alpha = 0$ [27], we get

$$\frac{\partial f}{\partial \alpha} = \frac{a\alpha}{(1 - \alpha)^2} + \frac{6b\alpha}{(1 - \alpha)^4} - 3\alpha^2 = 0. \tag{12}$$

The equilibrium is stable provided $\partial f(\alpha)/\partial \alpha < 0$. The structures will be instable or collapse onto the ground plate as $\partial f(\alpha)/\partial \alpha > 0$.

Comparing equations (11) and (12), and eliminating a, we obtain the nonlinear equation about the pull-in angle α_{PI} as

$$\left[\ln(1 - \alpha_{PI}) + \frac{\alpha_{PI}}{1 - \alpha_{PI}} \right] [3\alpha_{PI}(1 - \alpha_{PI})^5 - 6b(1 - \alpha_{PI})]$$
$$= \alpha_{PI}^2 [\alpha_{PI}(1 - \alpha_{PI})^3 - b(3 - \alpha_{PI})]. \tag{13}$$
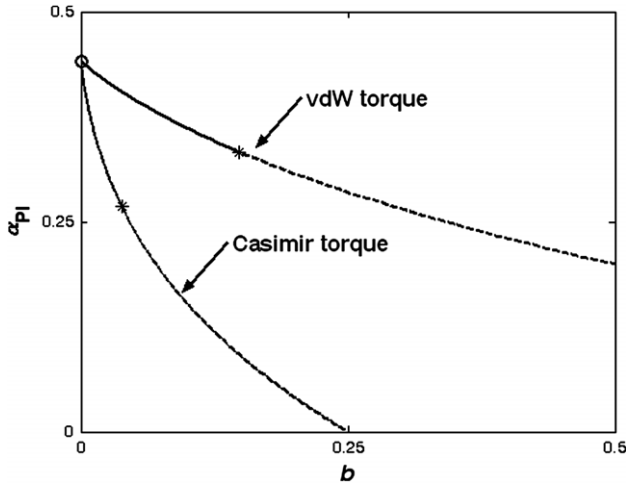
Figure 2. Comparison between the vdW and Casimir torques with variation of the pull-in gap α_{PI} with parameter b.

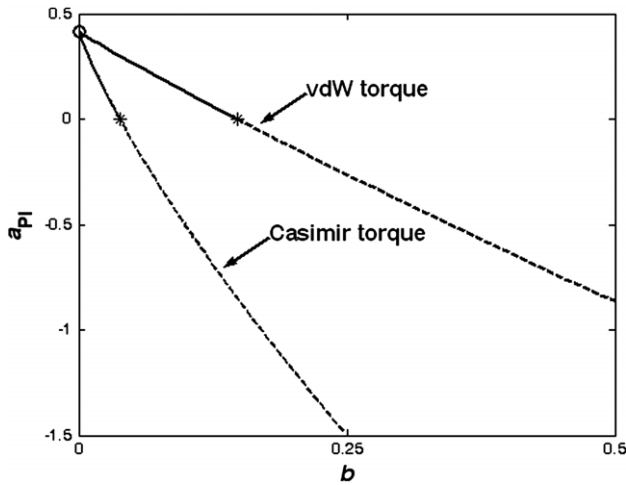**Figure 3.** Comparison between the vdW and Casimir torques with variation of the pull-in parameter a_{PI} with parameter b.

Substituting α_{PI} into equation (11), we get

$$a_{PI} = \alpha_{PI}^2 \frac{\alpha_{PI} - b \dfrac{3 - \alpha_{PI}}{(1 - \alpha_{PI})^3}}{\ln(1 - \alpha_{PI}) + \dfrac{\alpha_{PI}}{1 - \alpha_{PI}}}, \tag{14}$$

where the pull-in parameter $a_{PI} = \varepsilon_0 w L^3 V_{PI}^2/(2kg^3)$ is related to the pull-in voltage V_{PI}. Thus, we discuss the pull-in parameter a_{PI} instead of the pull-in voltage V_{PI} in this paper.

According to equation (13), we first plot the variation of the pull-in angle with parameter b in figure 2. The corresponding variation of the pull-in parameter a_{PI} with parameter b is shown in figure 3 according to equation (14). In these two figures, we should notice two special points which are plotted by '○' and '∗', respectively. The point '○' with the Casimir force corresponds to $(b_0, \alpha_0) = (0, 0.4404)$ in figure 2 and to $(b_0, a_0) = (0, 0.4137)$ in figure 3. This implies that there is no effect of the Casimir force on the varactor. In the presence of the Casimir torque, the pull-in angle α_{PI} and pull-in parameter a_{PI} decrease. At the other special point '∗' with the Casimir force, it corresponds to $(b^*, \alpha^*) = (0.0385, 0.2679)$
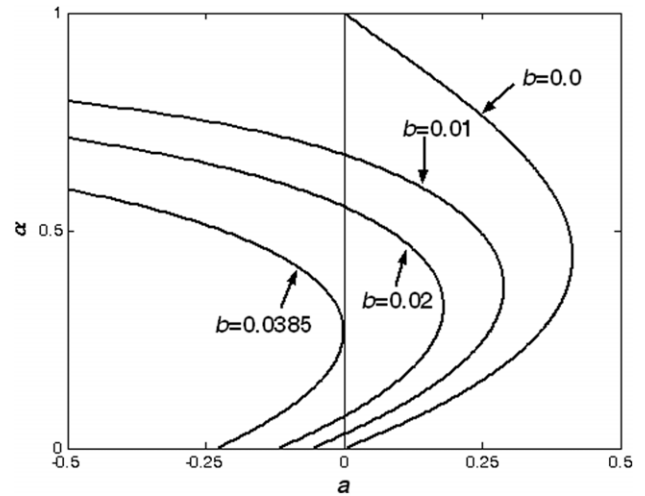

Figure 4. Variation of equilibrium points with parameter a for given different b with the Casimir torque.

in figure 2 and to $(b^*, a^*) = (0.0385, 0)$ in figure 3. That is, a will be negative when $b > b^*$. It implies the varactor will lose its stability even though there is no voltage applied at the torsional varactor.

2.3. Dynamical behaviour

The dynamical behaviour of equation (10) will be discussed in this section. Setting $\beta = \dot{\alpha}$, equation (10) can be transformed into the following form:

$$\begin{cases} \dfrac{d\alpha}{d\tau} = \beta, \\ I \dfrac{d\beta}{d\tau} = \dfrac{a}{\alpha^2} \left[\ln(1 - \alpha) + \dfrac{\alpha}{1 - \alpha} \right] + b \dfrac{3 - \alpha}{(1 - \alpha)^3} - \alpha \\ \qquad = \dfrac{f(\alpha, a, b)}{\alpha^2}. \end{cases} \tag{15}$$

The equilibrium points can be obtained by setting zero the left-hand sides of equation (15). The second equation of equilibrium points is equivalent to equation (11), which has two parameters a and b. Equation (11) can be solved numerically for α as a function of a and b. We plot the variation of α with parameter a for different values of parameter b; the solution is shown in figure 4. Since $a = \varepsilon_0 w L^3 V^2/(2kg^3)$ is non-negative, then the solution is physically meaningful when the solution curves are on the right of $a = 0$. So from this figure, we notice that equation (15) has one or two equilibrium points for $a \geqslant 0$ just when $0 < b < b^*$, otherwise there is no equilibrium point.

In order to check the stability of the equilibrium points, we need the Jacobian matrix of equation (15) as follows:

$$J = \begin{bmatrix} 0 & 1 \\ \dfrac{1}{\alpha^2} \left(\dfrac{\partial f}{\partial \alpha} - \dfrac{2f}{\alpha} \right) & 0 \end{bmatrix}. \tag{16}$$

We first discuss the stability of the equilibrium points with the given parameters $a = 0$ and $b < b^*$. According to figure 4, there are two equilibrium points $(\alpha_1, 0)$ and $(\alpha_2, 0)$ which satisfy the inequality $\alpha_1 < \alpha^* < \alpha_2$.
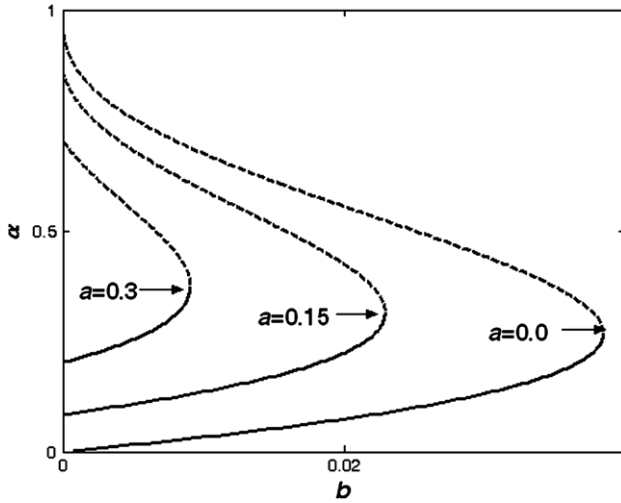
Figure 5. Bifurcation diagram: variation of equilibrium points with parameter b for given different a with the Casimir torque.

First, we consider the equilibrium point stability of the special state that there is no electrostatic torque on the upper torsional beam. Then substituting $a = 0$, $b < b^*$ and $\alpha = \alpha_1$ into equation (16), we get

$$J|_{\alpha=\alpha_1} = \begin{bmatrix} 0 & 1 \\ \dfrac{2b(4-\alpha_1)}{(1-\alpha_1)^4} - 1 & 0 \end{bmatrix}. \quad (17)$$

Since $b < b^*$ and $\alpha_1 < \alpha^*$, it follows that the corresponding eigenvalue equation of the Jacobian matrix has two pure imaginary roots, which means the equilibrium point $(\alpha_1, 0)$ is a Hopf bifurcation point. According to the property of the Hopf bifurcation point, this point is an equilibrium point. This means the restoring torque is equal to the Casimir torque, and the varactor keeps a balance state. When we add a small perturbation on the upper beam, then it will periodically oscillate around the equilibrium point. Subsequently, we take $a = 0$, $b < b^*$ and $\alpha = \alpha_2 > \alpha^*$ in equation (16) and solve its eigenvalue equation, and it has two real roots, of which one is positive and the other is negative. This means that the equilibrium point $(\alpha_2, 0)$ is an unstable saddle point. This means that the restoring torque still equals the Casimir torque; that is, the torsional varactor keeps the balance at the second state with the same a and b. However, when we add a small perturbation on the upper beam, it will reach the other equilibrium point (Hopf bifurcation point) or collapse onto the ground plate. This equilibrium state is unstable by definition.

Second, applying the same method to discuss the stability of the two solutions with any given different a and b, we can plot the bifurcation diagram as in figure 5. In figure 5, all the points of the real line (lower branch) represent the Hopf bifurcation point, and all the points of the dashed line (upper branch) are the unstable saddle point; the upper beam is unstable.

By the property of the Hopf bifurcation point and the unstable saddle point, there exist periodic orbits around the Hopf bifurcation point, but the periodic orbit will break into a homoclinic orbit meeting the unstable saddle point. In order to see the movement process of the equilibrium points, we
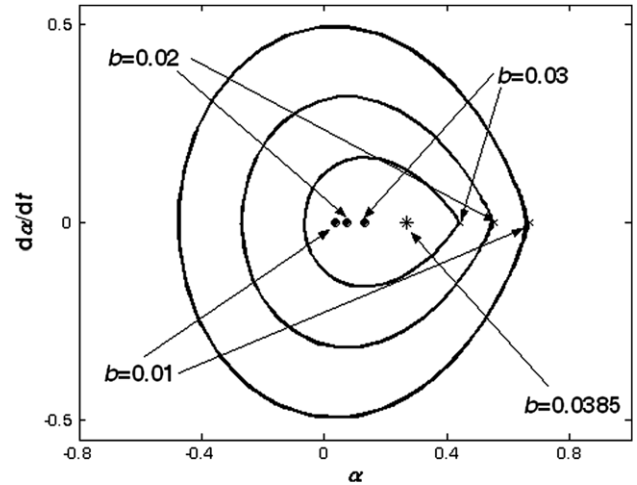
Figure 6. Phase diagram with different b for $a = 0$ with the Casimir torque.

can draw the phase portraits for different parameters b and for given $a = 0$ as shown in figure 6, from which, when b is equal to 0.01, 0.02 or 0.03, there are two equilibrium points, one is the Hopf bifurcation point (marked by '·') and the other is the unstable saddle point (marked by '×'). In the same manner, there is a homoclinic orbit passing through the unstable saddle point. We also note that the Hopf bifurcation point and the unstable saddle point move to the point '∗' from the opposite direction with b increasing. This point happens to be the pull-in point $(\alpha^*, d\alpha^*/dt) = (0.2679, 0)$ with the pull-in parameter $b^* = 0.0385$. At this critical condition, the pull-in phenomenon occurs; then we can find that the reason for structure invalidation is that the original two equilibrium points become one with the change in parameters.

3. Influence of van der Waals force

3.1. Mechanical model

Consider the same varactor shown in figure 1. When we consider the influence of the vdW force, there are still three forces in total, i.e. the restoring torque $M_{res}(\theta)$, the electrostatic torque $M_{elec}(\theta)$ and the vdW torque $M_{vdW}(\theta)$. The expression for the former two torques is the same as in section 2.1. Using the same method to compute the Casimir torque, we can get the vdW torque as follows:

$$M_{vdW}(\theta) = \int_0^L x \cdot dF_{vdW} = \frac{AwL^2}{12\pi g} \cdot \frac{1}{(g - L\theta)^2}. \quad (18)$$

We introduce six dimensionless variables; five of them are the same as in section 2.1, i.e. $\alpha = \theta/\theta_{max}$, $\theta_{max} = g/L$, $\tau = t/t_0$, $I = I_0/(kt_0^2)$ and $a = \varepsilon_0 w V^2 L^3/(2kg^3)$, and the new one $b = AwL^3/(12k\pi g^4)$ denotes the order of magnitude of ratio between the vdW and the restoring torques. Thus, the dimensionless form of the equation of motion $I_0\ddot{\theta} = M_{elec} + M_{vdW} - M_{res}$ is

$$I\frac{d^2\alpha}{d\tau^2} = \frac{a}{\alpha^2}\left[\ln(1-\alpha) + \frac{\alpha}{1-\alpha}\right] + \frac{b}{(1-\alpha)^2} - \alpha$$

$$= \frac{g(\alpha, a, b)}{\alpha^2}, \quad (19)$$

where

$$g(\alpha, a, b) = a\left[\ln(1-\alpha) + \frac{\alpha}{1-\alpha}\right] + \frac{b\alpha^2}{(1-\alpha)^2} - \alpha^3. \quad (20)$$

The solutions are physically meaningful in the region $0 < \alpha < 1$.

3.2. Pull-in parameters and dynamical behaviour

The equivalent equation $g(\alpha, a, b) = 0$ will be discussed in this section by setting zero the left-hand side of equation (19). Using the critical condition $\partial g(\alpha)/\partial \alpha = 0$ [27], we obtain the nonlinear equation for the pull-in angle α_{PI} as

$$(1 - \alpha_{\text{PI}})[3\alpha_{\text{PI}}(1-\alpha_{\text{PI}})^3 - 2b]\left[\ln(1-\alpha_{\text{PI}}) + \frac{\alpha_{\text{PI}}}{1-\alpha_{\text{PI}}}\right]$$
$$= \alpha_{\text{PI}}^2[\alpha_{\text{PI}}(1-\alpha_{\text{PI}})^2 - b], \quad (21)$$

and the pull-in parameter $a_{\text{PI}} = \varepsilon_0 w L V_{\text{PI}}^2/(2kg^3)$ as

$$a_{\text{PI}} = \alpha_{\text{PI}}^2 \frac{\alpha_{\text{PI}} - \dfrac{b}{(1-\alpha_{\text{PI}})^2}}{\ln(1-\alpha_{\text{PI}}) + \dfrac{\alpha_{\text{PI}}}{1-\alpha_{\text{PI}}}}. \quad (22)$$

According to equations (21) and (22), we can plot the variation of the pull-in angle and pull-in parameter a_{PI} with parameter b in figures 2 and 3, respectively. There are two special points as the points marked by '∘' and '∗' in figures 2 and 3. The point '∘' with the vdW torque corresponds to $(b_0, \alpha_0) = (0, 0.4404)$ in figure 2 and to $(b_0, a_0) = (0, 0.4137)$ in figure 3. This implies that there is no effect of the vdW force on the varactor. The point '∗' with the vdW torque corresponds to $(b^*, \alpha^*) = (4/27, 1/3)$ in figure 2 and to $(b^*, a^*) = (4/27, 0)$ in figure 3.

As in section 2.3, we transform equation (19) into the following form:

$$\begin{cases} \dfrac{\mathrm{d}\alpha}{\mathrm{d}\tau} = \beta, \\ I\dfrac{\mathrm{d}\beta}{\mathrm{d}\tau} = \dfrac{a}{\alpha^2}\left[\ln(1-\alpha) + \dfrac{\alpha}{1-\alpha}\right] + \dfrac{b}{(1-\alpha)^2} - \alpha \\ \qquad = \dfrac{g(\alpha, a, b)}{\alpha^2} \end{cases} \quad (23)$$

to discuss the dynamical behaviour with the vdW torque. This part of the discussion is quite similar to section 2.3, and we have the same kind of results. The dynamical system (23) has two equilibrium points, one of which is the Hopf bifurcation point and the other is the unstable saddle point. There are periodic orbits around the Hopf bifurcation point but they will break into a homoclinic orbit when meeting the unstable saddle point.

4. Conclusions

The influence of the Casimir and vdW forces on the nonlinear behaviour of the electrostatic torsional varactor is presented.

First, we study the variation of pull-in parameters α_{PI} and a_{PI} with parameter b and get two special points in figures 2 and 3 with the Casimir torque and the vdW torque, respectively. The first special point shows that there is no effect of the Casimir force or the vdW force on the varactor. The second

point shows that the varactor will lose its stability even though there is no voltage applied at the torsional varactor. With the appearance of the Casimir torque and the vdW torque, the pull-in parameters α_{PI} and a_{PI} all decrease. However, the corresponding critical parameter b^* is different; $b^* = 0.0385$ with the Casimir torque and $b^* = 4/27$ with the vdW torque. It means that the influence of the Casimir torque is stronger than that of the vdW torque for the same torsional varactor with the same geometry parameters. This result is consistent with [10].

Second, considering a and b as two parameters, we study the equilibrium points and their corresponding stability. No solution exists satisfying $a \geqslant 0$ in $0 < \alpha < 1$ when $b \geqslant b^*$. There are two equilibrium points for any $a \geqslant 0$ when $b < b^*$, of which one equilibrium point is a Hopf bifurcation point and the other is an unstable saddle point. There are periodic orbits around the Hopf bifurcation point and a homoclinic orbit passing through the unstable saddle point.

It should be noted that this paper only considered the ideal case for the Casimir force. Other influences such as materials, temperature and geometry can be introduced by equation (1) [23].

References

[1] Serry F M, Walliser D and Maclay G J 1998 *J. Appl. Phys.* **84** 2501
[2] Bukes E and Roukes M L 2001 *Phys. Rev.* B **63** 033402
[3] Chan H B, Aksyuk V A, Kleiman R N, Bishop D J and Capasso F 2001 *Science* **291** 1941
[4] Chan H B, Aksyuk V A, Kleiman R N, Bishop D J and Capasso F 2001 *Phys. Rev. Lett.* **87** 211801
[5] Bordag M, Mohideen U and Mostepanenko V M 2001 *Phys. Rep.* **353** 1
[6] Blencowe M 2004 *Phys. Rep.* **395** 159
[7] Dequesnes M, Rotkin S V and Aluru N R 2002 *Nanotechnology* **13** 120
[8] Lin W H and Zhao Y P 2003 *Chin. Phys. Lett.* **20** 2070
[9] Wang G W, Zhang Y, Zhao Y P and Yang G T 2004 *J. Micromech. Microeng.* **14** 1119
[10] Guo J G and Zhao Y P 2004 *J. Microelectromech. Syst.* **13** 1027
[11] Lin W H and Zhao Y P 2005 *Microsyst. Technol.* **11** 80
[12] Lin W H and Zhao Y P 2005 *Chaos, Solitons Fractals* **23** 1777
[13] Palasanzas G and DeHosson J Th M 2005 *Phys. Rev.* B **72** 121409
[14] Palasanzas G and DeHosson J Th M 2006 *J. Appl. Phys.* **99** 084906
[15] Palasanzas G and DeHosson J Th M 2005 *Phys. Rev.* B **72** 115426
[16] Palasanzas G 2006 *J. Adhes. Sci. Technol.* **20** 1321
[17] Guo J G and Zhao Y P 2006 *Int. J. Solids Struct.* **43** 675
[18] Ramezani A, Alasty A and Akbari J 2006 *Microsyst. Technol.* **12** 1153

[19] Esquivel-Sirvent R, Reyes L and Bárcenas J 2006 *New J. Phys.* **8** 241

[20] Zhao Y P, Wang L S and Yu T X 2003 *J. Adhes. Sci. Technol.* **17** 519

[21] Zhu J, Ru C Q and Mioduchowski A 2006 *J. Adhes. Sci. Technol.* **20** 1125

[22] Klimchitskaya G L, Mohideen U and Mostepanenko V M 2000 *Phy. Rev.* A **61** 062107

[23] Emig T and Buscher R 2004 *Nucl. Phys.* B **696** 468

[24] Emig T, Hanke A, Golestanian R and Kardar M 2003 *Phys. Rev.* A **67** 022114

[25] Venkatesh C, Pati S, Bhat N and Pratap R 2005 *Sensors Actuatuators* A **121** 480

[26] Degani O 1990 *J. Microelectromech. Syst.* **7** 373

[27] Seydel R 1994 *Practical Bifurcation and Stability Analysis: from Equilibrium to Chaos* 2nd edn (Berlin: Springer)